

## 2,2,2-Trichloro-*N*-({2-[2-(dimethylamino)ethyl]-1,3-dioxo-2,3-dihydro-1*H*-benzo[de]isoquinolin-5-yl}carbamoyl)acetamide (UNBS3157), a Novel Nonhematotoxic Naphthalimide Derivative with Potent Antitumor Activity

Eric Van Quaquebeke,<sup>†</sup> Tine Mahieu,<sup>†</sup> Patrick Dumont,<sup>†,‡</sup> Janique Dewelle,<sup>†</sup> Fabrice Ribaucour,<sup>†</sup> Gentiane Simon,<sup>†</sup> Sébastien Sauvage,<sup>†</sup> Jean-François Gaussin,<sup>†</sup> Jérôme Tuti,<sup>†</sup> Mohamed El Yazidi,<sup>†</sup> Frank Van Vynckt,<sup>†</sup> Tatjana Mijatovic,<sup>†</sup> Florence Lefranc,<sup>‡,§,⊥</sup> Francis Darro,<sup>†</sup> and Robert Kiss<sup>\*,‡,⊥</sup>

Unibioscreen SA, 40 Avenue Joseph Wybran, 1070 Brussels, Belgium, Laboratoire de Toxicologie, Institut de Pharmacie, Université Libre de Bruxelles, Brussels, Belgium, and Service de Neurochirurgie, Cliniques Universitaires de Bruxelles, Hôpital Erasme, Université Libre de Bruxelles, Brussels, Belgium

Received March 19, 2007

Amonafide (**1**), a naphthalimide which binds to DNA by intercalation and poisons topoisomerase II $\alpha$ , has demonstrated activity in phase II breast cancer trials, but has failed thus far to enter clinical phase III because of dose-limiting bone marrow toxicity. Compound **17** (one of 41 new compounds synthesized) is a novel anticancer naphthalimide with a distinct mechanism of action, notably inducing autophagy and senescence in cancer cells. Compound **17** (2,2,2-trichloro-*N*-({2-[2-(dimethylamino)ethyl]-1,3-dioxo-2,3-dihydro-1*H*-benzo[de]isoquinolin-5-yl}carbamoyl)acetamide (UNBS3157)) was found to have a 3–4-fold higher maximum tolerated dose compared to amonafide and not to provoke hematotoxicity in mice at doses that display significant antitumor effects. Furthermore, **17** has shown itself to be superior to amonafide in vivo in models of (i) L1210 murine leukemia, (ii) MXT–HI murine mammary adenocarcinoma, and (iii) orthotopic models of human A549 NSCLC and BxPC3 pancreatic cancer. Compound **17**, therefore, merits further investigation as a potential anticancer agent.

### Introduction

Isoquinolindione (naphthalimide) derivatives continue to be of interest because in addition to being DNA intercalators they have found application as fluorescent dyes and have some potential in the synthesis of polymers.<sup>1–3</sup> In therapeutics, naphthalimides have been evaluated for photodynamic therapy<sup>4</sup> and numerous derivatives have been evaluated as antitumor agents,<sup>5–9</sup> with a number, for example DMP840 (a bis-naphthalimide derivative) and amonafide (NSC-308847, nafi-dimide), a 5-amino-naphthalimide derivative, having reached clinical trials.<sup>10,11</sup> However, most have been abandoned because of a poor therapeutic index. Amonafide (**1**), which acts as a topoisomerase II poison,<sup>11–14</sup> has completed several phase I and phase II clinical trials. The compound has, however, with the exception of advanced breast cancer,<sup>15,16</sup> shown no activity or only limited activity against a range of different cancer types. Dose-limiting myelosuppression is also a key issue for the compound.<sup>17–21</sup> The compound's toxicity, which is highly variable, is linked to its metabolism. Amonafide can be metabolized by *N*-oxidation (via CYP1A2) to generate a rapidly eliminated inactive metabolite. Alternatively, it can be metabolized by the enzyme *N*-acetyltransferase 2 (NAT2) to *N*-acetyl-amonafide (**2**), a metabolite that is no longer a substrate for

CYP1A2, but displays in vitro cytotoxicity similar to that of amonafide.<sup>22</sup> The variability in the clinical toxicity of amonafide has been attributed to differential in vivo metabolism by NAT2. The enzyme is highly polymorphic and individuals can be classified, according to their metabolic activity, as slow or fast acetylators.<sup>23</sup> For most NAT2 substrates, toxic side effects are associated with the slow acetylator phenotype. Amonafide is an exception because it exhibits a significantly higher toxicity in fast acetylators than in slow acetylators.<sup>24,25</sup> Fast acetylator phenotypes lead to increased metabolism to *N*-acetyl amonafide, reduced oxidation of amonafide, and consequently, higher exposure to more toxic compounds for longer periods than is evident in slow acetylators.<sup>23–25</sup>

To minimize this toxicity, Chemgenex Pharmaceuticals (Grovedale, Victoria, Australia) and Xanthus (Cambridge, Massachusetts), who reinitiated the clinical development of amonafide, were obliged to first phenotype patients using caffeine as the NAT2 probe substrate to define slow and fast acetylators and then adjust amonafide clinical doses, accordingly. However, we have focused our efforts on synthesizing derivatives of naphthalimide, with improved antitumor activity and a significantly higher safety profile than amonafide. In addition to amonafide (**1**), *N*-acetyl-amonafide (**2**), and amonafide's nitro analog (**3**), 41 new naphthalimide derivatives (among which 39 have been described by our group in WO2005/105753 patent)<sup>26</sup> have been synthesized and evaluated because of their novelty in cancer models in vitro and in vivo.

### Chemistry

The synthesis of amonafide (**1**) was carried out according to a two-step process given in Figure 1.

The starting reactant used was the commercially available 3-nitro-1,8-naphthalic anhydride. The first step reaction proceeded with a 93% yield to furnish after filtration a yellow-

\* To whom correspondence should be addressed. Laboratoire de Toxicologie, Institut de Pharmacie, Université Libre de Bruxelles, Campus de la Plaine, CP205/1, Boulevard du Triomphe, 1050 Brussels, Belgium. Phone: +32 477 62 20 83. Fax: +32 23 32 53 35. E-mail: rkiss@ulb.ac.be.

<sup>†</sup> Unibioscreen SA.

<sup>‡</sup> Institut de Pharmacie, Université Libre de Bruxelles.

<sup>§</sup> Hôpital Erasme, Université Libre de Bruxelles.

<sup>⊥</sup> Current Address: Service d'Anatomie Pathologique, Cliniques Universitaires de Bruxelles, Hôpital Erasme, Université Libre de Bruxelles, Brussels, Belgium.

<sup>⊥</sup> R.K. is a Director of Research at the Belgian National Fund for Scientific Research (FNRS, Belgium). F.L. is a Clinical Research Fellow with the FNRS.

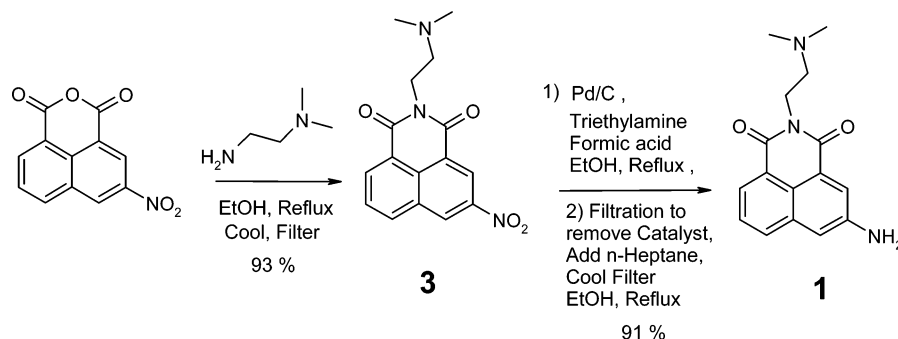


**Figure 1.** The two-step reaction to obtain the synthon amonafide (**1**) from commercially available 3-nitro-1,8-naphthalic anhydride.

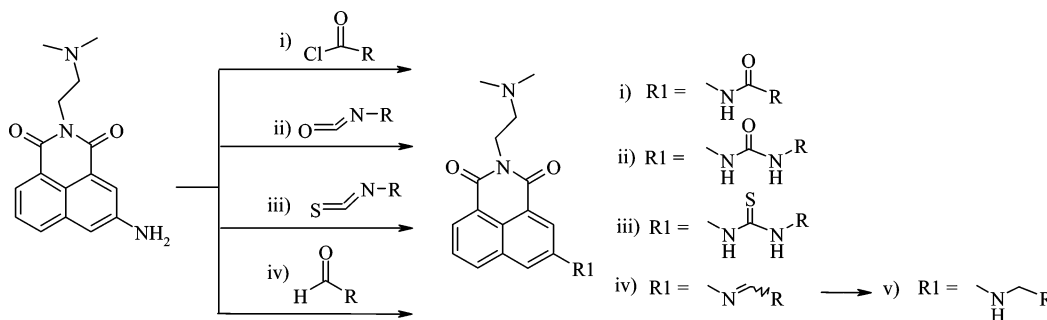


**Figure 2.** Schematic chemical modification to obtain new derivatives from amonafide (**1**) used as a synthon.

orange solid (**3**), with an HPLC-UV purity of 100% (a/a). The reduction of the nitro function to an amino (reaction 2) proceeded with a reasonable yield by Pd on carbon using triethylamine and formic acid in refluxing ethanol. After removing the catalyst by filtration, the addition of heptane was used to precipitate (**1**) as a yellow solid, which was produced with a 91% yield. The purity of the amonafide (**1**) was determined by HPLC-UV to be 100% (a/a). The global yield of the two steps was 84.6%. Detailed descriptions of these chemical steps are included in the Supporting Information (SI).

Our chemical strategy then focused on modifications to the aryl amino function of amonafide to render it less susceptible to interaction with NAT2, with the aim of reducing the potential toxicity of new analogues. A total of 44, additional naphthalimide derivatives were synthesized that can be divided into five distinct subclasses (Figure 2): (i) amides (obtained by reacting amonafide with different acyl chlorides), (ii) ureas (reacting amonafide with isocyanates), (iii) thioureas (reacting amonafide with isothiocyanates), (iv) imines (reacting amonafide with aldehydes), and (v) amines (by reduction of the imines previously obtained in iv).

The common synthon of all new derivatives generated in the current work was amonafide (**1**).

## Pharmacology

**Characterization of the In Vitro Cytotoxic Activity, In Vivo Maximum Tolerated Dose in Healthy Mice, and the In Vivo Antitumor Activity (L1210 Mouse Leukemia Model) of Synthesized Naphthalimide Derivatives.** Table 1 reveals that the most potent naphthalimide derivatives under study displayed in vitro antiproliferative activity ( $IC_{50}$  values from the MTT colorimetric assay) only in the  $\mu$ M range. Additionally, no statistically significant ( $p > 0.05$ ; Spearman rank correlation test) relationships between in vitro  $IC_{50}$  values, in vivo MTD values (tolerance) and in vivo antitumor activity in the L1210 mouse leukemia model (Table 1) were observed. This indicated that the most potent compounds in vitro were not always the most active in vivo (compounds **1**, **4**, **5**, **11**, **18**, **22**, etc;

Table 1). In the same manner, some apparently inactive or weakly active compounds in vitro displayed marked in vivo antitumor activity (**2**, **27**, **29**, **33**; Table 1). Collectively, these data suggested that in vitro testing of naphthalimide derivatives was not necessarily appropriate for identifying compounds with potent in vivo activity and low hematotoxicity.

Among the more active in vivo antitumor compounds (Table 1), that is, those associated with %T/C index values of  $\geq 200\%$ , some displayed higher toxicity: MTDs of  $\leq 40$  mg/kg (e.g.: **2**, **9**) compared to others, for example: **17**, **19**, **21**, **27**, **29**, **33**, and **35**, which had MTDs of  $\geq 80$  mg/kg. Table 1 also reveals that amonafide (**1**) was associated with weak in vivo activity in the L1210 leukemia model (T/C = 140%), while its toxic metabolite, *N*-acetyl-amonafide (**2**), displayed high activity. Of the 44 total naphthalimide derivatives evaluated in the course of the present study, four (**17**, **27**, **29**, **33**) were associated with marked in vivo activity (T/C values  $> 300\%$  or close to 300%) in the L1210 mouse leukemia model, with low in vivo toxicity (MTDs  $\geq 80$  mg/kg).

Accordingly, it was decided to more rigorously investigate the in vivo antitumor activity profiles of these four compounds in comparison to amonafide (**1**) and *N*-acetyl-amonafide (**2**) in the L1210 mouse leukemia model. Table 2 indicates that amonafide in the dose range 2.5 to 20 mg/kg i.p. was associated with weak in vivo antitumor activity, with %T/C values ranging between 109 and 143% when administered four times a week for two consecutive weeks on days 1–4 and 8–11 post-L1210 cell injection to mice on day 0. Higher doses of **1** were toxic. Under an identical regimen, the *N*-acetyl derivative of amonafide (**2**) displayed marked in vivo antitumor activity, but with a very narrow therapeutic window (Table 2). Of the four novel naphthalimide derivatives, **17**, **27**, **29**, and **33**, investigated, **17** demonstrated consistently high %T/C values 200–300% over the dose range 10–160 mg/kg i.p. and the highest therapeutic window (Table 2). These data prompted investigation whether the higher therapeutic window of certain of these naphthalimide

Table 1. Compounds Synthesized, Their In Vitro Cytotoxic Activity, and Their In Vivo Activity and Tolerance

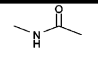
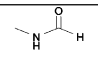
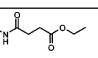
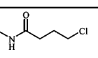
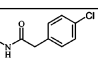
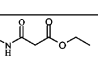
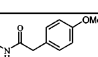
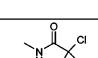
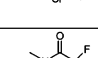
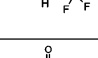
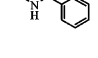
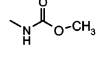
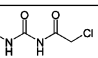
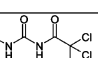
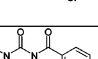
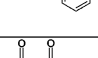
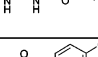
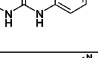
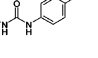
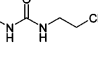
R <sub>1</sub>	Compo und number	In Vitro Cytotoxicity IC <sub>50</sub> <sup>a</sup> (μM)							In Vivo MTD <sup>b</sup> (mg/kg)	In Vivo L1210 Activity	
		Hs683	U373-MG	HCT-15	LoVo	A549	MCF-7	Mean ± SEM		T/C (%)	Doses (mg/kg)
NO <sub>2</sub>	3	3.7	1.3	2.6	0.4	2.4	-	2.1 ± 0.6	40	193	20
NH <sub>2</sub>	1	3.9	3.5	5.2	2.7	3.8	5.8	4.1 ± 0.5	40	140	5
H	4	6.9	7.5	9.2	4.7	5.6	10.0	7.3 ± 0.8	40	156	80
NH <sub>2</sub> .HCl	5	4.7	4.5	8.8	3.5	4.8	9.0	5.9 ± 1.0	-	120	10
	2	>10.0	9.0	7.8	>10.0	>10.0	>10.0	<sup>c</sup>	40	> 300	20
	6	4.8	4.4	4.3	6.6	3.9	7.4	5.2 ± 0.6	>80	ND	ND
	7	>10.0	>10.0	>10.0	>10.0	>10.0	>10.0	<sup>c</sup>	>80	156	80
	8	>10.0	>10.0	>10.0	10.0	>10.0	>10.0	<sup>c</sup>	>80	164	80
	9	7.0	5.8	5.5	4.8	4.7	4.8	5.4 ± 0.4	20	200	10
	10	>10.0	>10.0	>10.0	>10.0	>10.0	>10.0	<sup>c</sup>	>80	129	10
	11	4.2	2.7	2.8	1.3	3.2	2.2	2.7 ± 0.4	10	107	10
	12	>10.0	8.9	>10.0	6.4	10.0	>10.0	<sup>c</sup>	>80	150	20
	13	8.7	8.1	>10.0	4.5	9.5	9.6	<sup>c</sup>	40	124	40
	14	5.6	6.0	8.4	3.7	8.5	>10.0	<sup>c</sup>	40	167	20
	15	3.3	4.2	7.2	4.1	5.9	>10.0	<sup>c</sup>	40	133	40
	16	3.0	3.3	4.5	2.9	4.1	4.9	3.8 ± 0.3	20	147	20
	17	0.8	0.9	0.9	0.9	0.9	1.8	1.0 ± 0.2	>160	> 300	80
	18	3.0	3.4	3.4	2.1	2.0	3.6	2.9 ± 0.3	40	140	40
	19	3.6	4.1	4.4	7.7	4.9	6.3	5.2 ± 0.6	80	207	40
	20	2.8	3.6	3.1	2.0	1.9	2.4	2.6 ± 0.3	80	161	80
	21	5.0	0.9	9.7	4.2	3.5	3.1	4.4 ± 1.2	>80	207	80
	22	4.6	1.0	5.6	1.8	3.0	3.9	3.3 ± 0.7	>80	156	20
	23	2.1	2.1	7.4	1.5	1.6	3.1	3.0 ± 0.9	>80	187	80
	24	5.8	1.4	7.7	4.4	5.5	6.6	5.2 ± 0.9	>80	187	80

Table 1. (Continued)

R <sub>1</sub>	Compound number	In Vitro Cytotoxicity IC <sub>50</sub> <sup>a</sup> (μM)							In Vivo MTD <sup>b</sup>	In Vivo L1210 Activity	
	25	2.6	3.1	5.8	3.2	3.1	6.5	4.1 ± 0.7	>80	194	80
	26	5.0	3.6	4.6	2.8	3.6	4.8	4.1 ± 0.4	40	124	20
	27	>10.0	>10.0	9.0	8.3	>10.0	>10.0	<sup>c</sup>	80	288	80
	28	>10.0	>10.0	>10.0	>10	>10.0	>10.0	<sup>c</sup>	>80	164	80
	29	>10.0	7.8	>10.0	8.4	9.1	>10.0	<sup>c</sup>	>160	> 300	80
	30	>10.0	6.4	>10.0	5.0	6.7	>10.0	<sup>c</sup>	>80	107	80
	31	>10.0	4.2	9.9	4.1	7.7	7.4	<sup>c</sup>	>80	135	80
	32	4.9	4.7	4.3	3.7	3.9	6.3	4.7 ± 0.4	40	210	40
	33	>10.0	5.0	>10.0	>10.0	>10.0	>10.0	<sup>c</sup>	>160	> 300	80
	34	9.8	>10.0	8.2	4.8	8.5	>10.0	<sup>c</sup>	>80	140	40
	35	4.5	4.0	4.5	3.7	>10	>10.0	<sup>c</sup>	>80	207	80
	36	>10.0	>10.0	>10.0	>10.0	>10.0	>10.0	<sup>c</sup>	>80	113	80
	37	>10.0	>10.0	>10.0	>10.0	>10.0	>10.0	<sup>c</sup>	>80	129	40
	38	>10.0	>10.0	>10.0	8.1	>10.0	>10.0	<sup>c</sup>	>80	157	80
	39	7.6	>10.0	8.0	5.0	>10.0	>10.0	<sup>c</sup>	>80	150	80
	40	5.5	7.1	6.7	4.0	9.7	8.9	7.0 ± 0.9	>80	150	80
	41	6.4	3.6	5.9	4.0	4.3	4.8	4.8 ± 0.4	40	171	80
	42	>10.0	>10.0	>10.0	>10.0	>10.0	>10.0	<sup>c</sup>	>80	178	178
	43	>10.0	>10.0	>10.0	8.7	>10.0	>10.0	<sup>c</sup>	>80	164	80
	44	>10.0	9.4	>10.0	>10.0	>10.0	>10.0	<sup>c</sup>	>80	147	147

<sup>a</sup> The in vitro antiproliferative activities of the 44 compounds are reported as IC<sub>50</sub> values (in μM), determined using the MTT colorimetric assay on culturing cancer cells in the presence of each drug for three days. These were determined in the six human cancer cell lines: Hs683 and U373-MG glioblastoma, HCT-15 and LoVo colon cancers, MCF-7 breast cancer, and A549 non-small-cell lung cancer. <sup>b</sup> In vivo tolerance was determined as the maximum tolerated dose (MTD in mg/kg), which represents the dose just below the lowest dose level that killed at least one mouse in a treatment group after a maximum of 28 days. <sup>c</sup> The mean IC<sub>50</sub> value could not be determined, as one or more of the corresponding data points were higher than the threshold value.

**Table 2.** %T/C Survival Indices for L1210 Leukemia-Bearing Mice after Treatment with Selected Naphthalimides<sup>a</sup>

dose level (i.p.; mg/kg)	compd 1 %T/C indices	compd 2 %T/C indices	compd 17 %T/C indices	compd 27 %T/C indices	compd 29 %T/C indices	compd 33 %T/C indices
2.5	109	nt <sup>b</sup>	nt <sup>b</sup>	nt <sup>b</sup>	nt <sup>b</sup>	nt <sup>b</sup>
5	143*	111	nt <sup>b</sup>	nt <sup>b</sup>	nt <sup>b</sup>	nt <sup>b</sup>
10	122	149*	197**	115	151*	215
20	121	300*** <sup>c</sup>	205**	150*	148*	195
40	49 <sup>d</sup>	48 <sup>d</sup>	272***	165*	232**	278
80	nt <sup>b</sup>	47 <sup>d</sup>	300*** <sup>c</sup>	295***	300*** <sup>c</sup>	300*** <sup>c</sup>
120	nt <sup>b</sup>	nt <sup>b</sup>	281***	41 <sup>d</sup>	42 <sup>d</sup>	40 <sup>d</sup>
160	nt <sup>b</sup>	nt <sup>b</sup>	300*** <sup>c</sup>	nt <sup>b</sup>	nt <sup>b</sup>	nt <sup>b</sup>

<sup>a</sup> \*:  $p < 0.05$ ; \*\*:  $p < 0.01$ ; \*\*\*:  $p < 0.001$ . The compounds were evaluated at specific dose levels in the range 2.5–160 mg/kg, dictated by their individual MTD values (Table 1). Compounds were administered i.p. four times a week for two consecutive weeks (days 1–4 and 8–11), with treatment starting the day following leukemia cell grafting into the mice (day 0). There were five mice per experimental group, and the potential therapeutic benefits contributed by each compound are evaluated by means of the T/C index. When a compound is associated with a T/C index value equal to 300%, it is considered to bring L1210 leukemia-bearing mice to the status of “long survivors”. <sup>b</sup> nt: not tested. <sup>c</sup> ls: long survivors. <sup>d</sup> t: toxic;  $p < 0.01$ .

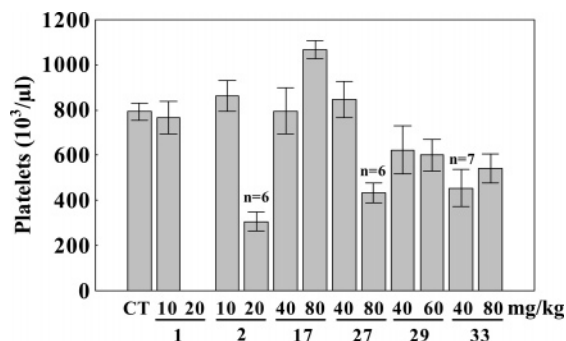


**Figure 3.** Determination of the potential hematotoxicity of compounds **1**, **2**, **17**, **27**, **29**, and **33**. This was assessed in terms of platelet numbers, in healthy mice receiving 15 i.p. administrations: three per week on Mondays, Wednesdays, and Fridays over five consecutive weeks. Each compound was evaluated at two distinct dose levels. “ $n = x$ ” is the number of mice from groups of 10 that survived the 15 administrations. The data are presented as mean values  $\pm$  SEM.

derivatives: **17**, **27**, **29**, and **33** offered a more favorable hematotoxicity profile than **1** (amonafile) or **2** (*N*-acetyl-amonafile).

**Compound 17 Displays Weaker Hematotoxicity in Healthy Mice than Amonafide and *N*-Acetyl-amonafile.** Groups of healthy mice (10 per group) received **1** (amonafile), **2**, **17**, **29**, or **33** three times a week (on Mondays, Wednesdays, and Fridays) for five consecutive weeks. Each compound was evaluated at two distinct doses, as detailed in Figure 3 and its legend. The groups were sacrificed 3 days following the last dose and blood samples were taken for determination of platelet, red blood cell (RBC), and white blood cell (WBC) counts. Figure 3 shows that the mice tolerated 15 chronic administrations of **1** and **2** at 10 mg/kg, while all animals died before receiving the complete set of 15 administrations of **1** at 20 mg/kg. Four of the 10 mice receiving 20 mg/kg of **2** also died before the end of the experiment, and the remaining six mice displayed a marked decrease in their platelet numbers (Figure 3). The present experiment, therefore, perfectly reproduced the known hematotoxicity of amonafile (**1**) and *N*-acetyl-amonafile (**2**).<sup>17–21</sup> Compounds **27**, **29**, and **33** also displayed significant ( $p < 0.05$  to  $p < 0.001$ ) decreases in platelet numbers compared to controls (Figure 3). In addition, **29** provoked severe decreases in RBC counts (data not shown). The only naphthalimide derivative studied that displayed no hematotoxicity (including not only platelet but also RBC {data not shown} and WBC {data not shown} counts) was **17** (Figure 3). Additional experiments have been performed with chronic oral and i.v. treatment of **17**. The data are provided in SI as Table 3. At high doses, **17** decreases the number of red blood cells and white blood cells, but not the number of platelets (see Table 3 in SI).

**Compound 17 Displays Similar or Higher In Vivo Antitumor Activity than Amonafide (**1**).** Of the multiple clinical trials that have been carried out with amonafile (**1**) or that are still ongoing, the most interesting data have been obtained in breast cancer.<sup>15,16</sup> For this reason, the antitumor activity of **17** (10 mg/kg i.v.) was first compared with that of **1** (10 mg/kg i.v.; Figure 4A) and taxol (20 mg/kg i.v.; Figure 4B) in the human MDA-MB-231 s.c. breast cancer model and then at a dose of 160 mg/kg i.p. against **1** (20 mg/kg i.p.) in the syngeneic s.c. mouse mammary MXT-HI cancer model (Figure 4C). The MXT tumor originates from the mammary galactophorous ducts and its MXT-HI variant is hormone-insensitive and highly metastasizing to the liver (the arrow in Figure 4D points to a large liver metastasis) when the primary tumor is grafted subcutaneously onto female B6D2F1 mice.<sup>27,28</sup>

Figure 4A shows that **1** and **17** displayed similar in vivo antitumor activity in their ability to decrease the growth rates of human MDA-MB-231 breast cancer xenografts. The MDA-MB-231 growing subcutaneously does not metastasize. Figure 4B shows that the in vivo antitumor activity of **17** (and, therefore, of **1**) was similar to that of taxol in this human MDA-MB-231 breast cancer xenograft model. These results for **17** must be considered with respect to the significant antitumor activity observed for **1** and taxol in breast cancer patients.<sup>15,16</sup> The experimental schedule used for taxol treatment in this MDA-MB-231 breast cancer xenograft model was chosen on the basis of optimized protocols published previously by Kraus-Berthier et al.,<sup>29</sup> with respect to the use of taxol in human xenograft models.

Figure 4C shows that **1** and **17** displayed weak in vivo antitumor activity in terms of their ability to reduce the growth rates of mouse MXT-HI mammary tumors, which heavily metastasizes to the liver (Figure 4D). In contrast, MXT-HI-tumor-bearing mice treated with **17** survived significantly ( $p < 0.01$ ) longer ( $T/C = 183\%$ ) than those treated with **1** ( $T/C = 143\%$ ), a feature that may suggest higher antimetastatic effects for **17** than for **1** in this mouse mammary tumor model. We are currently investigating this hypothesis at the experimental level.

**Compound 17 Displays Similar or Higher In Vivo Antitumor Activity than Irinotecan and Gemcitabine in Models of Human NSCLC and Pancreatic Cancer, Respectively.** Figure 5A shows that **17** (10 mg/kg i.v.) significantly increased the survival of A549 NSCLC orthotopic xenograft-bearing mice, while **1** (amonafile) at the same dose level did not. The activity of **17** in this A549 NSCLC orthotopic xenograft model was of the same magnitude as that contributed by irinotecan (Figure 5B). Figure 5Ca morphologically illustrates the almost total destruction of the lung parenchyma by the A549 NSCLC

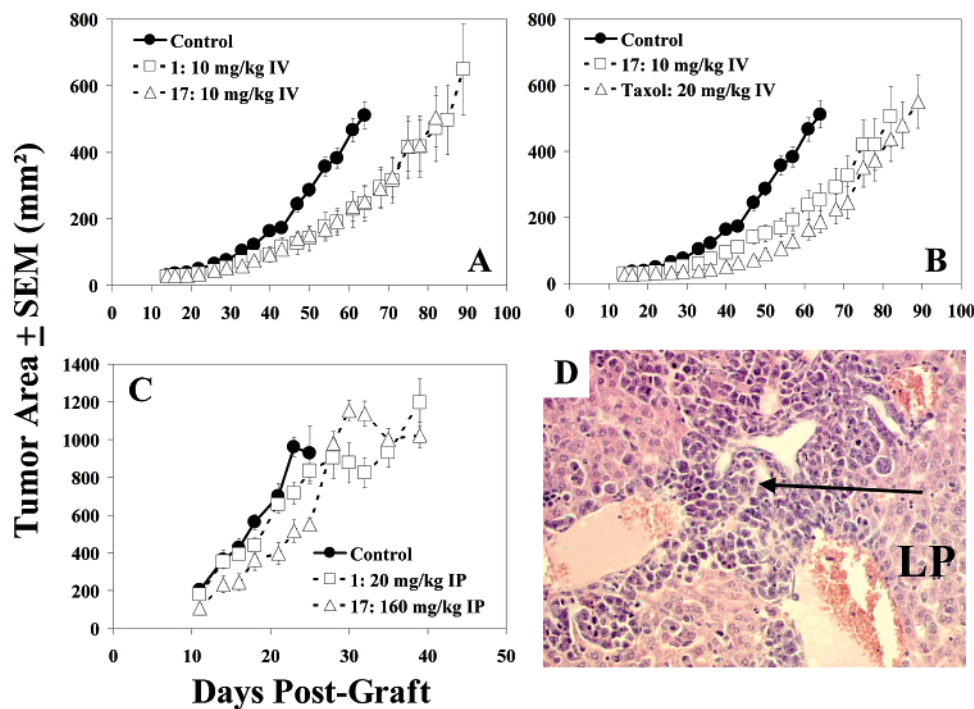


**Figure 4.** Compound-induced changes in tumor surface area ( $\text{mm}^2$ ) in s.c. models of human breast and mouse mammary cancers. (A) Immuno-compromised mice implanted s.c. with human MDA-MB-231 breast cancer cells and treated i.v. with **1** (amonaflide) or **17**. (B) Immuno-compromised mice implanted s.c. with human MDA-MB-231 breast cancer cells and treated i.v. with taxol or **17**. (C) Immuno-competent mice implanted s.c. with mouse MXT-H1 mammary adenocarcinoma and treated i.p. with **1** or **17**. For A–C, compounds **1** and **17** were administered using a schedule of five successive injections per week for three weeks, with drug administration starting on day 14 post-tumor graft. Taxol was administered using a schedule of one injection per week for three weeks, with drug administration starting on day 14 post-tumor graft. Each experimental group contained nine animals. The data are presented as mean values  $\pm$  SEM. The control group is the same in Figures 4A and 4B. (D) Morphological illustration (HE staining;  $G \times 200$ ) of a large MXT-H1 mammary tumor metastasis (to which the black arrow points) developing in liver parenchyma (LP).

orthotopic xenograft one month after grafting A549 cells into the lungs. This A549 NSCLC orthotopic xenograft model gives brain (Figure 5Cb) and liver (data not shown) metastases in more than 80% of A549 NSCLC-bearing immuno-compromised mice.<sup>30</sup> Compound **17** (20 mg/kg i.v.) also showed similar activity to gemcitabine (40 mg/kg i.v.; Figure 5D) in the orthotopic BxPC3 pancreas cancer model (Figure 5Da), which also gives prominent liver metastases (Figure 5Db).

**Compound 17 Is Not a Topoisomerase II Poison.** Amonafide<sup>31</sup> and amonafide derivatives<sup>32–35</sup> intercalate with DNA and poison topoisomerase II $\alpha$ . The ability of **17** to act as a DNA intercalator was, thus, first compared with that of **1** and **29** (which displays similar in vitro and in vivo antitumor effects to **17** (Table 1), but has higher hematotoxic effects (Figure 3)). DNA unwinding tests were performed using eukaryotic topoisomerase I (Figure 6A). The method is based on the ability of topoisomerase I to negatively supercoil a relaxed plasmid in the presence of a DNA intercalating agent. In a topoisomerase I-containing reaction, the presence of a DNA unwinding/intercalating agent will lead to the formation of a relaxed “underwound” DNA molecule with a deficient linking number. Upon removal of the intercalating agent, this relaxed “underwound” molecule converts to a supercoiled molecule, owing to the recovery of the normal DNA twist. Figure 6A shows representative results of such experiments in which the reactions are performed in the presence of increasing concentrations of the molecules to determine the  $UC_{50}$  of the test compounds. The  $UC_{50}$  is the drug concentration at which the relaxed band is shifted to the midpoint between the supercoiled and the relaxed states. The results indicate that both **29** (Figure 6Ab) and **17** (Figure 6Ac) are able to intercalate with DNA. Under

our experimental conditions, amonafide (**1**) had a  $UC_{50}$  of 8  $\mu\text{M}$  (Figure 6Aa) and that determined for **29** was similar at 13  $\mu\text{M}$  (Figure 6Ab). In contrast, **17** had a higher  $UC_{50}$  ( $\sim 40 \mu\text{M}$ ), which means a higher drug concentration is required to induce the same topoisomerase II shift toward the supercoiled form. Compounds **17** and **29** were then investigated to determine whether they act as topoisomerase II poisons. Topoisomerase II regulates DNA topology via a breakage–reunion cycle; an activity necessary for the segregation of interlocked chromosomes at mitosis and the removal of excess supercoiling generated during processes such as replication or transcription.<sup>36</sup> After interacting noncovalently with DNA, topoisomerase II simultaneously cuts both DNA strands and a covalent intermediate is then established between each subunit of the topoisomerase II homodimer and the newly created DNA 5'-phosphate ends via phosphotyrosyl bonds.<sup>36</sup> This transient intermediate is called the cleavable complex because disruption of the catalytic cycle at this stage results in a permanent protein-associated DNA double-stranded break. Under normal conditions, cleavable complexes are rapidly converted back to noncleavable forms and, therefore, they exist at a very low steady-state in cells.<sup>36</sup> However, a number of antitumor drugs are able to induce a drastic increase in the number of topoisomerase II–DNA covalent intermediates that are present in a cell at a given time by inhibiting the religation step and by enhancing the rate of cleavage. Ultimately, this situation results in an accumulation of double-stranded DNA breaks and cell death. Thus, topoisomerase II poisons convert the protein into an intracellular toxin whose action damages the genome.<sup>36</sup>

An in vitro plasmid-based system was used to determine the ability of test compounds to act as topoisomerase II poisons.

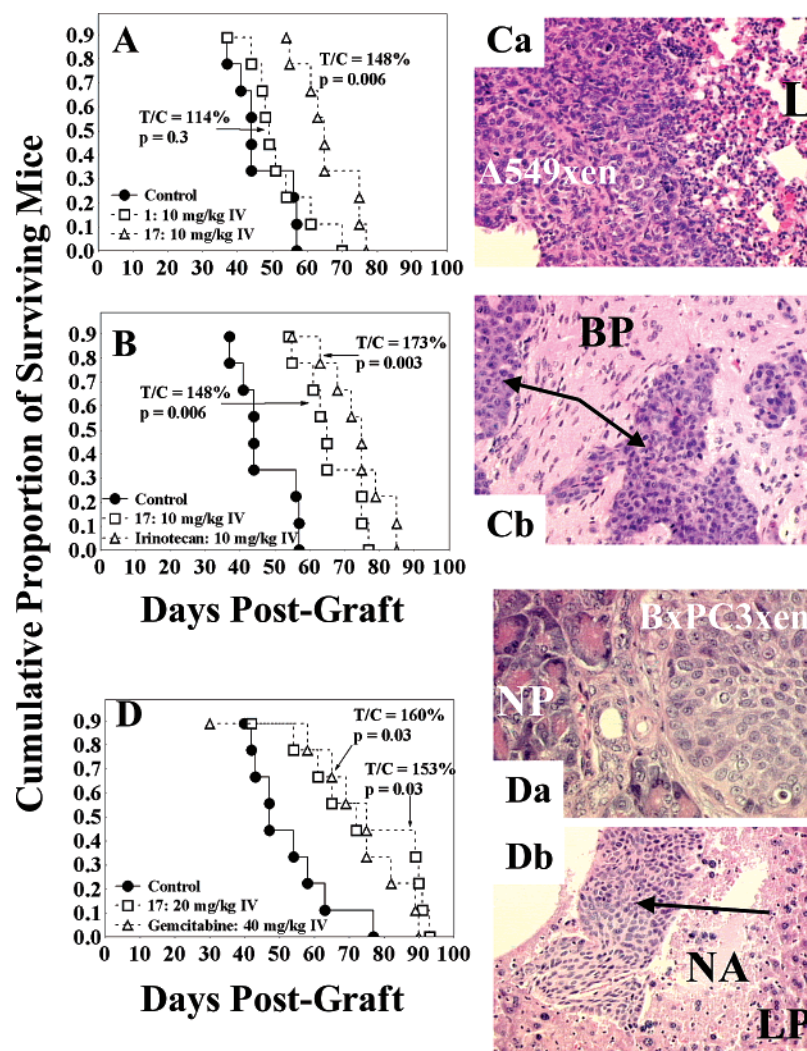


**Figure 5.** Compound activity in orthotopic models of human lung and pancreatic cancer. (A) The activity of i.v. administered **1** or **17** on the survival of mice orthotopically grafted with human A549 NSCLC. (B) The activity of i.v. administered **17** or irinotecan on the survival of mice orthotopically grafted with human A549 NSCLC. (Ca) Typical morphological illustration (HE staining;  $G \times 100$ ) of the development of a human A549 NSCLC xenograft (A549xen) in the lung parenchyma (L) of an immuno-compromised mouse. This mouse was orthotopically grafted with A549 tumor cells one month earlier. (Cb) Typical morphological illustration (HE staining;  $G \times 100$ ) of the development of human A549 NSCLC xenograft metastases (see the black arrows) in the brain parenchyma (BP) of an immuno-compromised mouse one month after A549 cell grafting into its lungs. (D) The activity of i.v. administered **17** and gemcitabine on the survival of mice orthotopically grafted with human BxPC3 pancreatic cancer. (Da) Typical morphological illustration (HE staining;  $G \times 200$ ) of the development of a human BxPC3 xenograft (BxPC3xen) in the normal pancreas (NP) of an immuno-compromised mouse. This mouse was orthotopically grafted with BxPC3 cells two months earlier. (Db) Typical morphological illustration (HE staining;  $G \times 100$ ) of the development of a BxPC3 metastasis (see the black arrow) in the liver parenchyma (LP) of an immuno-compromised mouse two months after BxPC3 cell grafting into its pancreas. Large areas of necrosis (NA) are induced by this metastatic process (Figure 5Db). Plots A, B, and D display the survival of the mice ( $n = 9$ ) in each group expressed as the decreasing cumulative proportion of those surviving (Kaplan–Meier survival analysis). The control group is the same in Figures 5A and 5B.

This assay measures the conversion of a covalently closed supercoiled plasmid into linear molecules as a consequence of stabilization of cleavable complexes leading to plasmid double-strand breaks. As shown in Figure 6B, compounds were tested at concentrations ranging from 6 to 100  $\mu\text{M}$ . The results obtained indicated that **29** (Figure 6Ba) is a topoisomerase II poison that is at least as potent as amonafide (**1**; Figure 6Ba) and its metabolite *N*-acetyl-amonafide (**2**; Figure 6Bb). For each of these compounds, 50  $\mu\text{M}$  was the concentration required for an optimal stabilization of the cleavable complex. Compound **17** did not act as a topoisomerase II poison in this assay (Figure 6Ba). Indeed, when compared to the control reaction performed in the absence of test compounds, no increase in the intensity of the linear band was observed after treatment with **17** (Figure 6Ba).

Various intercalating agents also have the ability to inhibit the strand-passage activity of topoisomerase II, in turn preventing the enzyme's ability to catalyze the double-strand cleavage of DNA and the passage of a second DNA duplex through the transiently established break. Accordingly, test compounds were also evaluated in the classical kinetoplast DNA (kDNA) decatenation assay.<sup>37</sup> Kinetoplast DNA is found in the mitochondria of protozoa and consists mainly of a large network of interlocked (catenated) mini-DNA circles of about 2.5 kb each. Topoisomerase II is able to decatenate this network into free mini-circles. Compounds **1**, **17**, and **29** were tested at 50  $\mu\text{M}$  for their ability to inhibit topoisomerase II-mediated kDNA decatenation. Compounds **17** and **29** as well as amonafide (**1**) inhibited this specific activity of topoisomerase II. Thus, although **17** does not seem to act as a topoisomerase II poison

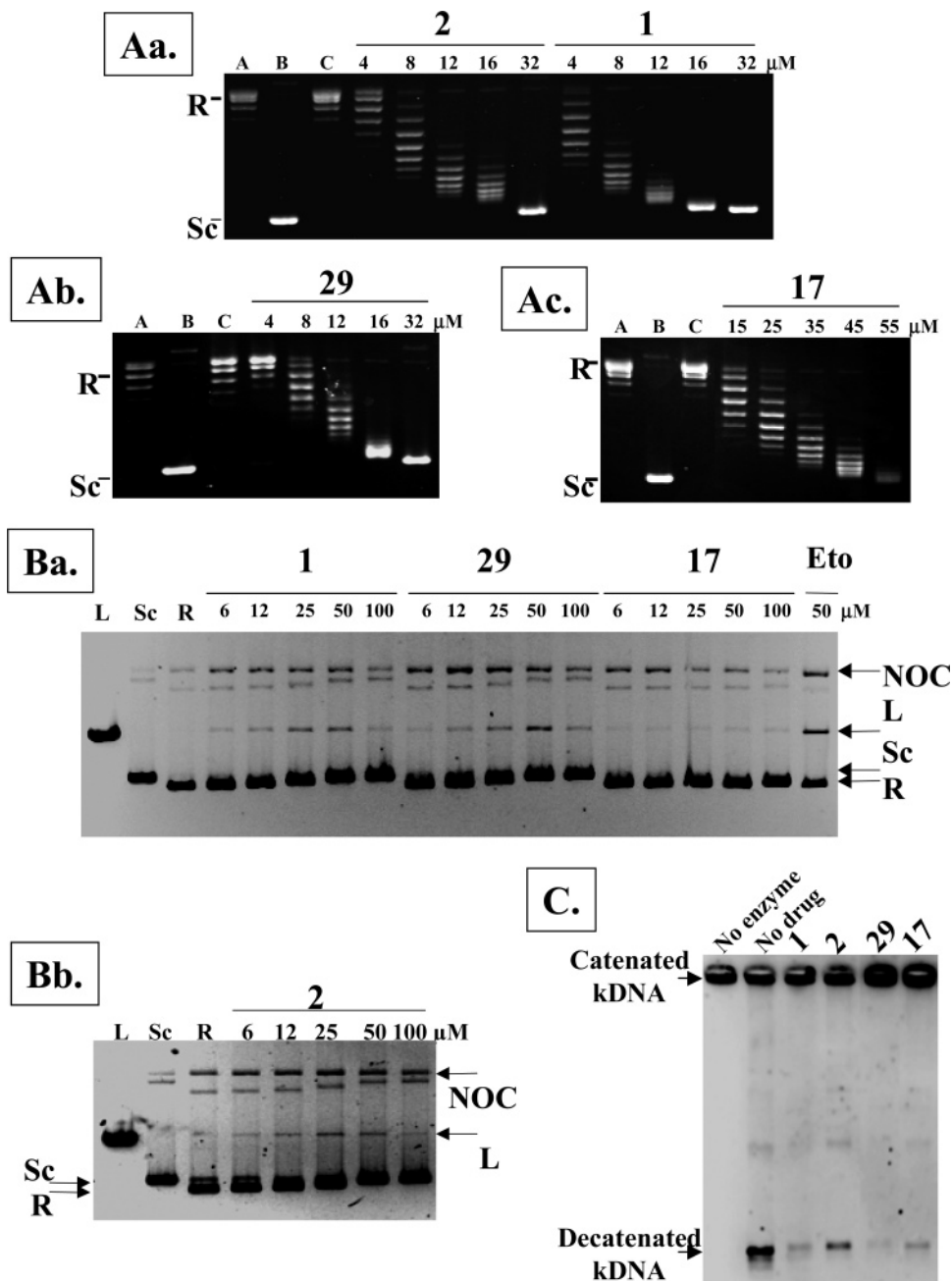


**Figure 6.** Ability of amonafide (1), *N*-acetyl amonafide (2), UNBS3157 (17), and 29 to act as DNA intercalating agents and to interfere with topoisomerase II activity. (A) The new amonafide derivatives are DNA intercalating agents of various potencies. Intercalation was monitored by conversion of relaxed pBR322 plasmid to supercoiled molecules, in the presence of topoisomerase I. Shown here are pictures of ethidium bromide stained agarose gels displaying the results of unwinding experiments for each molecule tested. Molecules were included in the reactions at final concentrations ranging from 4 to 32  $\mu\text{M}$ , except for 17 (15–55  $\mu\text{M}$ ). The position of the supercoiled (Sc) and relaxed (R) pBR322 forms is indicated on each gel. A: substrate (relaxed pBR322); B: supercoiled pBR322 (marker); C: control reaction performed in the absence of test compounds, but with the addition of solvent alone (DMSO). (B) UNBS3157 (17) does not cause pBR322 linearization in the presence of topoisomerase II $\alpha$ . The stimulation of topoisomerase II-dependent DNA cleavage is observed by an increase in the intensity of the linear pBR322 band (L), corresponding to an enhancement of cleavable complex stabilization. In these reactions, supercoiled pBR322 was relaxed in the presence of 10 units of topoisomerase II $\alpha$ . Amonafide (Ba), its *N*-acetylated metabolite (Bb), as well as 17 (Ba) and 29 (Ba) were tested at various concentrations, ranging from 6 to 100  $\mu\text{M}$ . Etoposide (Eto, Ba), a well-known topo II poison, was used as a positive control at a concentration of 50  $\mu\text{M}$ . L: linear marker (pBR322 digested with Eco RI); Sc: supercoiled marker (no enzyme reaction); R: relaxed marker (control reaction in the presence of solvent but without added test compounds). Arrows indicate the positions of the relaxed (R), the supercoiled (Sc), the linear (L), and the nicked open circular (NOC) forms. (C) The inhibition of topoisomerase II strand-passage activity was measured by a kDNA decatenation assay. Catenated kDNA remains localized in the wells due to the large size of the network, while decatenated kDNA is able to enter the gel. An agarose gel stained with ethidium bromide is shown. The test compounds were evaluated in the reactions at a concentration of 50  $\mu\text{M}$  (no enzyme: negative decatenation control; and no drug: positive decatenation control).

(Figure 6B), it is, however, able to inhibit its strand-passage activity (Figure 6C). Additional results indicate that none of the tested molecules inhibit the strand-passage activity of topoisomerase I even at high concentrations (data not shown).

**Compound 17 Does Not Induce Apoptosis in Human PC-3 and DU-145 Prostate Cancer Cells, but Does Induce Autophagy and Senescence.** A hallmark of topoisomerase II-targeting drugs is the induction of apoptosis. This is the



consequence of an intracellular increase in the level of DNA damage provoked by stabilization of the cleavable complex and a failure to achieve complete chromosome segregation as a result of inhibition of topoisomerase II strand-passage activity.<sup>36</sup> Amonafide and amonafide analogues, that is, R16, are topoisomerase II inhibitors that induce apoptosis.<sup>32</sup> Flow cytometry was used to determine the percentage of human PC-3 and DU-145 prostate cancer cells that underwent apoptosis (i.e., positive for both Annexin V and propidium iodide) when treated with **17**. It was observed that only ~10% of PC-3 (the gray bars) and up to 15–20% DU-145 (the black bars) cells underwent apoptotic processes following treatment with **17** at 10  $\mu$ M (Figure 7Aa).

Compound **17** failed to induce activation of p53 in PC-3 cells, which is a p53-deleted cell line (Figure 7Ab).<sup>38</sup> DU-145 cells express constitutively higher levels of p53 (Figure 7Ab), which is typical of cells containing mutant p53 compared to human MCF-7 breast cancer cells (Figure 7Ba) that express wild-type p53.<sup>39,40</sup> p53 was indeed constitutively activated in DU-145 cells and **17** did not further activate p53 (Figure 7Ab). Adriamycin (ADR) was chosen as a positive control for p53 activation in MCF-7 breast cancer cells (Figure 7Ba). While both **1** and **29** markedly activated p53 in MCF-7 cells, **17** did not (Figure 7Bb). The absence of clear **17**-induced apoptosis in PC-3 and DU-145 prostate cancer cells was further evidenced by the absence of any procaspase-3 and -9 activation and also by the absence of clear PARP cleavage in both PC-3 and DU-145 prostate cancer cells treated with **17** (Figure 7Ab). Taken together, these data appear to rule out a potential pro-apoptotic effect for **17**.

However, pro-autophagic effects were observed in PC-3 and to a markedly lesser extent in DU-145 cells treated with **17** (Figures 7Ca and 7Cb). This was initially assessed by the quantification of acidic vesicular organelles, including autophagic vacuoles in compound-treated cells using acridine orange staining (Figure 7Ca). The percentage of cells with positive red staining increased from approximately 5 to 35% in PC-3 cells treated for 72 h with 10  $\mu$ M of **17** (gray bars in Figure 7Ca). The maximum of autophagic DU-145 cells did not exceed 10% with the same treatment (Figure 7Ca). Second, cellular changes in the expression of LC3 (a specific autophagy marker; Figure 7Cb) on treatment with **17** were assessed.<sup>41,42</sup> LC3 is microtubule-associated protein 1 light chain 3, which is the autophagosomal orthologue of yeast *Atg8/Aup7*.<sup>41–44</sup> In untreated control cells, LC3 type I (LC3-I) and LC3 type II (LC3-II) were expressed at higher levels in DU-145 than in PC-3 cells (Figure 7Cb); a feature that could at least partly explain why **17** induced less pro-autophagic effects in DU-145 compared to PC-3 cells (Figure 7Ca). Drug-induced pro-autophagic effects are paralleled by a significant increase in the percentages of cells in the G2 phase of the cell cycle.<sup>43</sup> This feature was clearly observed when PC-3 cells were treated for 72 h with 10  $\mu$ M of **17** (the upper panel in Figure 7Da) but not when DU-145 cells were treated in the same manner (the lower panel in Figure 7Da).

Compound **17** seems to induce autophagy in PC-3 cells but not in DU-145 cells, while the reverse feature has been observed with respect to senescence. Using SA- $\beta$ -galactosidase staining, a specific marker for senescence,<sup>45,46</sup> it was observed that DU-145 cells treated for 72 h with 10  $\mu$ M **17** underwent marked processes of senescence, while PC-3 cells did so but to a markedly lesser extent (Figure 7Db). A moderate concentration (20 nM) of adriamycin (ADR) was used as the positive control (Figure 7Db) to induce senescence in wild-type as well as p53-mutated human cancer cells.<sup>47</sup> As indicated above, PC-3 cells are p53-null not p53-mutated (Figure 7Ab), a feature that could

therefore explain, at least partly, why both ADR and **17** failed to induce marked senescence in PC-3 cells, while they both did in DU-145 cells (Figure 7Db). Indeed, agents that induce telomere shortening can also trigger a cell to enter senescence.<sup>44,46</sup> In this case, a senescence program is initiated that induces the activation of various cell-cycle inhibitors and reduces the function of p53.<sup>44,46</sup> It has been confirmed that compound **17** does not shorten PC-3 telomeres (data not shown).

## Discussion

Naphthalimides, a class of compounds that bind to DNA by intercalation have shown high anticancer activity against a variety of murine and human tumor cells.<sup>48</sup> Two representatives, mitonafide and amonafide, were evaluated in clinical trials as potential anticancer agents.<sup>48</sup> The therapeutic properties of these initial lead drugs have been improved by designing bisintercalating agents.<sup>49–51</sup> One of these, elinafide, which has shown marked in vitro and in vivo activity, has also been evaluated in clinical trials against solid tumors.<sup>48,52</sup>

In the present study, it has been demonstrated that compound **17**, obtained in three chemical steps from commercially available 3-nitro-1,8-naphthalic anhydride, is a novel anticancer naphthalimide<sup>26</sup> with in vitro antiproliferative activity (IC<sub>50</sub> range of 0.8–1.8  $\mu$ M) against human cancer cell lines, including glioblastoma (Hs683 and U373-MG), colorectal (HCT-15 and LoVo), non-small-cell lung cancer (A549), and breast cancer (MCF-7), similar to that of amonafide (**1**: IC<sub>50</sub> range of 2.7–5.8  $\mu$ M), which has reached clinical phase II and demonstrated activity notably in breast cancer.<sup>15,16</sup> Amonafide (**1**) has failed thus far to enter phase III because of dose-limiting bone marrow toxicity, leading to thrombocytopenia, anemia, and leukopenia, which is linked to its metabolism (via a polymorphic enzyme, *N*-acetyltransferase 2) to a toxic metabolite, *N*-acetyl-amonafide.<sup>23–25</sup> Compound **17** (2,2,2-trichloro-*N*-({2-[2-(dimethylamino)ethyl]-1,3-dioxo-2,3-dihydro-1*H*-benzo[de]isoquinolin-5-yl}carbonyl)acetamide (UNBS3157)) has been designed to avoid the metabolism that provokes the clinical hematotoxicity of amonafide. Accordingly, in mice, compound **17** was found to have a 3–4-fold higher maximum tolerated dose compared to **1** irrespective of administration route and to provoke significantly weaker hematotoxicity in mice than **1**. Furthermore, **17** has shown itself to be superior to **1** in vivo in models of (i) L1210 murine leukaemia, (ii) MXT-HI murine mammary adenocarcinoma (note the improved %*T/C* values in the Experimental Section), and (iii) orthotopic models of human A549 NSCLC and BxPC3 pancreas cancer.

Preliminary data indicate that the mechanism of action of **17** is in part different to that of **1**, which is described as a DNA intercalating agent and topoisomerase II poison.<sup>11–14</sup> Compound **17** demonstrates 5-fold weaker intercalating activity than **1**, and although able to inhibit topoisomerase II-mediated kinetoplast DNA decatenation, it does not appear to be a topoisomerase II poison, unlike **1**. Furthermore, in breast carcinoma cells, **17** does not induce rapid, marked, and sustained up-regulation of p53, unlike **1**, and it does not induce type I programmed cell death (apoptosis) as the result of its antitumor activity. In contrast, **17** induces type II programmed cell death (autophagy) in human p53-null prostate cancer cells (PC-3 cell line), but not in, or only weakly so, human p53-mutated (but still functional) prostate cancer cells (DU-145 cell line). In contrast, compound **17** induces senescence (cell proliferation arrest) in the p53-mutated DU-145 prostate cancer cells, but does not do so, or only induces this effect to a markedly lower extent, in p53-null PC-3 cells. Compound **17** displays antiproliferative activity

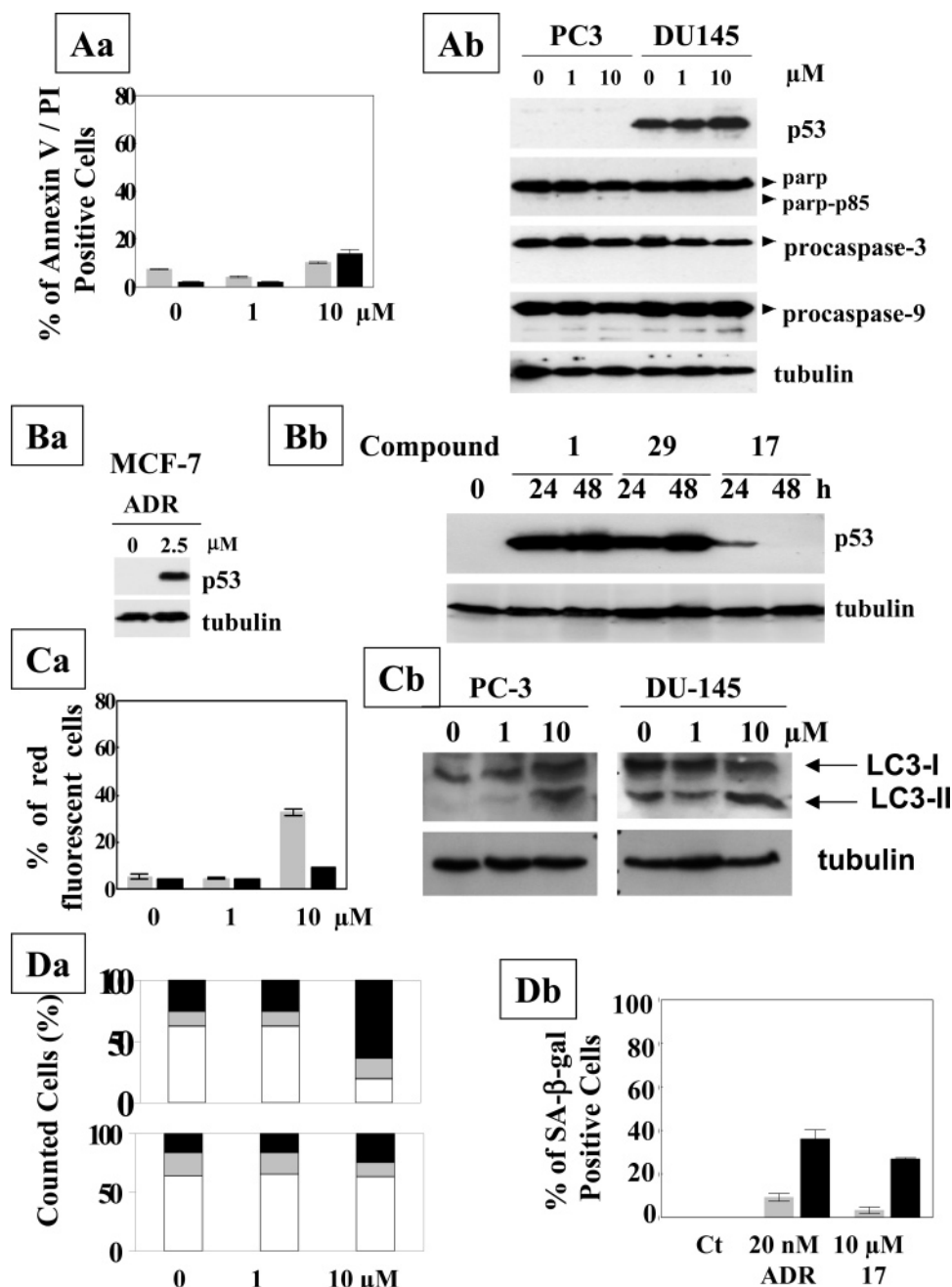


**Figure 7.** UNBS3157 (**17**) does not induce apoptosis but has potent pro-autophagic effects or induces senescence in specified human prostate cancer cells. (Aa) Drug-induced apoptotic effects as evaluated by flow cytometry with Annexin V-FITC staining of PC-3 (gray bars) or DU-145 (black bars) prostate cancer cells after treatment for 72 h with 0 (Ct: untreated cells), 1, or 10 μM UNBS3157 (compound **17**). (Ab) Immunoblotting determination of UNBS3157 (**17**)-induced effects on p53, PARP, procaspase-3, and procaspase-9 expression and activation in PC-3 and DU-145 cells. UNBS3157 effects were evaluated over 72 h at 1 and 10 μM in comparison to untreated (Ct) cells. (Ba) Adriamycin (ADR; 2.5 μM for 24 h) was chosen as a positive control for p53 activation in MCF-7 breast cancer cells. (Bb) Immunoblotting evaluation of 20 μM amonafide (which is known to intercalate DNA and poison topoisomerase IIα) and UNBS3157 (compound **17**) effects on p53 activation in MCF-7 human breast cancer cells. Tubulin immunoblotting was used as a loading control. (Ca) Drug-induced pro-autophagic effects as evaluated by quantification of acidic vesicular organelles (revealed as red fluorescent staining), following acridine orange staining of PC-3 (gray bars) or DU-145 (black bars) cells after treatment for 72 h with 0 (Ct, untreated cells), 1, or 10 μM UNBS3157 (**17**). (Cb) Cell lysates of PC-3 and DU-145 cells treated for 72 h with 1 and 10 μM UNBS3157 (**17**) were analyzed by Western blotting for LC3-I/II expression using an antibody kindly provided by Dr. Yasuko Kondo (MD Anderson Cancer Center, Houston, TX). (Da) Drug-induced effects on the cell cycle as evaluated by propidium iodide (PI) staining of PC-3 (upper panel) or DU-145 (lower panel) human prostate cancer cells after they had been treated for 72 h with 0 (Ct, untreated cells), 1, or 10 μM UNBS3157 (**17**). Cell cycle phases are divided into G2/M phase (black bars), S phase (gray bars), and G0/G1 phase (white bars). (Db) Quantification of the induction of senescence-associated β-galactosidase activity in PC-3 and DU-145 cells following 10 μM UNBS3157 (**17**) treatment for 72 h. Adriamycin (ADR; 20 nM) was used as the positive control in these experiments. The results are expressed as the percentage of senescence-associated β-galactosidase positive staining.

against a wide range of different human cancer cells, but it appears that the nature of its anticancer effects (i.e., autophagy versus senescence) may be dependent on the status of p53 in these cancer cells.

It must be remembered that cancer cells, in their relentless drive to survive, hijack many normal processes including cell cycle signaling, angiogenesis, glucose metabolism, apoptotic cell death, and multidrug resistance mechanisms, all mechanisms

in which p53 exerts more or less an important role. Induction of autophagic cell death and senescence has clear clinical potential in treating cancers with apoptotic defects.<sup>41–44,53</sup> Glioblastomas and melanomas are typical examples of cancers that are resistant to apoptosis.<sup>54,55</sup> Temozolomide, a pro-autophagic drug, shows promising therapeutic benefits in the context of these two types of cancers.<sup>43,54–56</sup> Other apoptosis-resistant cancers, including NSCLCs and pancreatic cancers, warrant intensive investigation with pro-autophagic drugs.<sup>30,57,58</sup>

In conclusion, the novel naphthalimide **17**, which has a distinct mechanism of action in comparison to amonafide, also displays in vivo higher antitumor activity in a range of cancer models and higher tolerance and significantly weaker hematotoxicity at “therapeutic” doses. Compound **17** therefore merits further investigation as a potential anticancer agent.

## Experimental Section

**Chemistry.** The chemical modifications to amonafide that have been realized are summarized in Table 1 and are described in greater detail in the SI.

**Pharmacology. In Vitro Pharmacology: Cell Lines.** Human cancer cell lines were obtained from the American Type Culture Collection (ATCC, Manassas, U.S.A.), the European Collection of Cell Culture (ECACC, Salisbury, U.K.), and the Deutsche Sammlung von Mikroorganismen und Zellkulturen (DSMZ, Braunschweig, Germany). The eight cell lines evaluated were the Hs683 (ATCC code HTB-138) and U373-MG (ECACC code 89081403) glioblastomas, the HCT-15 (DSMZ code ACC357) and LoVo (DSMZ code ACC350) colon cancer, the A549 (DSMZ code ACC107) non-small-cell-lung cancer (NSCLC), the MCF-7 (DSMZ code ACC115) breast cancer, and the PC-3 (ATCC code CRL1435) and DU145 (ATCC code HTB81) prostate cancer models.

**Evaluation of In Vitro Cell Proliferation by Means of the MTT Colorimetric Assay.** The overall growth level of the human cancer cell lines was then determined by means of the colorimetric MTT (3-[4,5-dimethylthiazol-2-yl]-diphenyl tetrazolium bromide, Sigma, Belgium) assay, as detailed previously.<sup>59–62</sup>

**In Vivo Testing. Maximum Tolerated Dose.** The acute maximum tolerated dose (MTD) was determined following single i.p. administration of increasing drug doses to groups of three healthy B6D2F1 female mice. Seven dose levels of each drug (2.5, 5, 10, 20, 40, 80, and 160 mg/kg) were evaluated. The MTD was defined as the dose just below the lowest dose level that killed at least one mouse in a treatment group after a maximum of 28 days.<sup>28,61</sup>

**Hematological Analyses in Healthy Mice.** Healthy B6D2F1 female mice (10 per group) received each compound i.p. using a schedule of three administrations per week for five consecutive weeks at two specified dose levels relative to their MTD. For drug administration, the compounds were solubilized in DMSO/saline (5:95 v/v). The mice were sacrificed 3 days post-final drug administration, blood was collected, and hematological profiling was undertaken by determining platelet, red blood cell (RBC), and white blood cell (WBC) counts using a Coulter Counter T-890 (Coulter Electronics, U.S.A.).

**In Vivo Evaluation of Antitumor Activity.** The details of each treatment are provided in the Experimental Section and also form part of the legends to the figures. The rest of the information is provided in the SI. The potential survival gain obtained using naphthalimide derivatives was evaluated by means of the %T/C index for the L1210 leukemia model<sup>28,63</sup> and by means of survival curve analyses for human orthotopic xenografts.<sup>30,62,64</sup> The %T/C index is the ratio of the median survival time of the treated animal group (*T*) and that of the control group (*C*). Toxic effects are indicated by %T/C indices of <75%. The benefit of chemotherapy is considered to be significant when associated with %T/C indices >130% (see Statistical Analyses).

**Biochemical and Molecular Biology Related Experiments.** All the experimental protocols are detailed in the SI.

**Statistical Analyses.** A statistical comparison of the control and treated groups was initially undertaken with the Kruskal–Wallis test (a nonparametric one-way analysis of variance). Where this revealed significant differences, the Dunn multiple comparison procedure (two-sided test) was applied. However, this was adapted to the special case of comparing treatment and control groups in which only (*k* – 1) comparisons were undertaken among the *k* groups tested by the Kruskal–Wallis test (instead of the possible *k*(*k* – 1)/2 comparisons considered in the general procedure). The levels of statistical significance associated with the %T/C survival indices were determined by using Gehan’s generalized Wilcoxon test. A correlation between the numerical variables was analyzed by means of the nonparametric Spearman correlation test. All these statistical analyses were carried out using Statistica (Statsoft, Tulsa, Oklahoma).

**Acknowledgment.** The present work was financially supported by grants awarded by the “Région de Bruxelles-Capitale” (Brussels, Belgium).

**Supporting Information Available:** Methods, experimental protocols, and <sup>1</sup>H NMR, <sup>13</sup>C NMR, ESIMS or EIMS, and IR spectral data. This material is available free of charge via the Internet at <http://pubs.acs.org>.

## References

- Vazquez, M. E.; Blanco, J. B.; Salvadori, S.; Trapella, C.; Argazzi, R.; Bryant, S. D.; Jinsmaa, Y.; Lazarus, L. H.; Negri, L.; Giannini, E.; Lattanzi, R.; Colucci, M.; Balboni, G. 6-*N,N*-Dimethylamino-2,3-naphthalimide: A new environment-sensitive fluorescent probe in delta- and mu-selective opioid peptides. *J. Med. Chem.* **2006**, *49*, 3653–3658.
- Flores, L. V.; Staples, A. M.; Mackay, H.; Howard, C. M.; Uthe, P. B.; Sexton, J. S., 3rd.; Buchmueller, K. L.; Wilson, W. D.; O’Hare, C.; Kluzza, J.; Hochhauser, D.; Hartley, J. A.; Lee, M. Synthesis and evaluation of an intercalator-polyamide hairpin designed to target the inverted CCAAT box 2 in the topoisomerase IIalpha promoter. *ChemBioChem* **2006**, *7*, 1722–1729.
- Niu, C. G.; Qin, P. Z.; Zeng, G. M.; Gui, X. Q.; Guan, A. L. Fluorescence sensor for water in organic solvents prepared from covalent immobilization of 4-morpholinyl-1,8-naphthalimide. *Anal. Bioanal. Chem.* **2007**, *387*, 1067–1074.
- Pervaiz, S. Reactive oxygen-dependent production of novel photochemotherapeutic agents. *FASEB J.* **2001**, *15*, 612–617.
- Chen, S. F.; Behrens, D. L.; Behrens, C. H.; Czerniak, P. M.; Dexter, D. L.; Dusak, B. L.; Fredericks, J. R.; Gale, K. C.; Gross, J. L.; Jiang, J. B.; et al. XB596, a promising bis-naphthalimide anticancer agent. *Anticancer Drugs* **1993**, *4*, 447–457.
- Bousquet, P. F.; Brana, M. F.; Conlon, D.; Fitzgerald, K. M.; Perron, D.; Cocchiari, C.; Miller, R.; Moran, M.; George, J.; Quian, X. D.; et al. Preclinical evaluation of LU79553: A novel bis-naphthalimide with potent antitumor activity. *Cancer Res.* **1995**, *55*, 1176–1180.
- Bailly, C.; Qu, X.; Chaires, J. B.; Colson, P.; Houssier, C.; Ohkubo, M.; Nishimura, S.; Yoshinari, T. Substitution at the F-ring N-imide of the indolocarbazole antitumor drug NB-506 increases the cytotoxicity, DNA binding, and topoisomerase I inhibition activities. *J. Med. Chem.* **1999**, *42*, 2927–2935.
- Li, Z.; Yang, Q.; Qian, X. Novel thiazonaphthalimides as efficient antitumor and DNA photocleaving agents: Effects of intercalation, side chains, and substituent groups. *Bioorg. Med. Chem.* **2005**, *13*, 4864–4870.
- Noel, G.; Godon, C.; Fernet, M.; Giocanti, N.; Megnin-Chanet, F.; Favaudon, V. Radiosensitization by the poly(ADP-ribose) polymerase inhibitor 4-amino-1,8-naphthalimide is specific of the S phase of the cell cycle and involves arrest of DNA synthesis. *Mol. Cancer Ther.* **2006**, *5*, 564–574.
- Thompson, J.; Pratt, C. B.; Stewart, C. F.; Avery, L.; Bowman, L.; Zamboni, W. C.; Pappo, A. Phase I study of DMP840 in pediatric patients with refractory solid tumors. *Invest. New Drugs* **1999**, *16*, 45–49.
- Andersson, B. S.; Beran, M.; Bakic, M.; Silberman, L. E.; Newman, R. A.; Zwelling, L. A. In vitro toxicity and DNA cleaving capacity of benzoquinolinedione (nafidimide; NSC 308847) in human leukemia. *Cancer Res.* **1987**, *47*, 1040–1044.
- Hsiang, Y. H.; Jiang, J. B.; Liu, L. F. Topoisomerase II-mediated DNA cleavage by amonafide and its structural analogs. *Mol. Pharmacol.* **1989**, *36*, 371–376.
- Bear, S.; Remers, W. A. Computer simulation of the binding of amonafide and azonafide to DNA. *J. Comput.-Aided Mol. Des.* **1996**, *10*, 165–175.

- (14) Wang, H.; Mao, Y.; Zhou, N.; Hu, T.; Hsieh, T. S.; Liu, L. F. Atp-bound topoisomerase II as a target for antitumor drugs. *J. Biol. Chem.* **2001**, *276*, 15990–15995.
- (15) Scheithauer, W.; Ditttrich, C.; Kornek, G.; Haider, K.; Linkesch, W.; Gisslinger, H.; Depisch, D. Phase II study of amonafide in advanced breast cancer. *Breast Cancer Res. Treat.* **1991**, *20*, 63–67.
- (16) Costanza, M. E.; Berry, D.; Henderson, I. C.; Ratain, M. J.; Wu, K.; Shapiro, C.; Duggan, D.; Kalra, J.; Berkowitz, I.; Lyss, A. P. Amonafide: an active agent in the treatment of previously untreated advanced breast cancer. A cancer and leukemia group B study (CALGB8642). *Clin. Cancer Res.* **1995**, *1*, 699–704.
- (17) O'Dwyer, P. J.; Paul, A. R.; Hudes, G. R.; Walczak, J.; Ozols, R. F.; Comis, R. L. Phase II study of amonafide (nafidamide, NSC 308847) in advanced colorectal cancer. *Invest. New Drugs* **1991**, *9*, 65–67.
- (18) Linke, K.; Pazdur, R.; Abbruzzese, J. L.; Ajani, J. A.; Winn, R.; Bradof, J. E.; Daugherty, K.; Levin, B. Phase II study of amonafide in advanced pancreatic adenocarcinoma. *Invest. New Drugs* **1991**, *9*, 353–356.
- (19) Perez, R. P.; Nash, S. L.; Ozols, R. F.; Comis, R. L.; O'Dwyer, P. J. Phase II study of amonafide in advanced and recurrent sarcoma patients. *Invest. New Drugs* **1992**, *10*, 99–101.
- (20) Malviya, V. K.; Liu, P. Y.; Alberts, D. S.; Surwit, E. A.; Craig, J. B.; Hannigan, E. V. Evaluation of amonafide in cervical cancer, phase II. A SWOG study. *Am. J. Clin. Oncol.* **1992**, *15*, 41–44.
- (21) Gallion, H. H.; Liu, P. Y.; Alberts, D. E.; O'Toole, R. V.; O'Sullivan, J.; Mills, G.; Smith, H. O.; Hynes, H. E. Phase II trial of amonafide in previously treated patients with advanced ovarian cancer: A Southwest Oncology Group study. *Gynecol. Oncol.* **1992**, *46*, 230–232.
- (22) Felder, T. B.; McLean, M. A.; Vestal, M. L.; Lu, K.; Farquhar, D.; Legha, S. S.; Shah, R.; Newman, R. A. Pharmacokinetics and metabolism of the antitumor drug amonafide (NSC-308847) in humans. *Drug Metab. Dispos.* **1987**, *15*, 773–778.
- (23) Ratain, M. J.; Mick, R.; Berezin, F.; Janisch, L.; Schilsky, R. L.; Vogelzang, N. J.; Lane, L. B. Phase I study of amonafide dosing based on acetylator phenotype. *Cancer Res.* **1993**, *53*, 2304–2308.
- (24) Ratain, M. J.; Mick, R.; Berezin, F.; Janisch, L.; Schilsky, R. L.; Williams, S. F.; Smiddy, J. Paradoxical relationship between acetylator phenotype and amonafide toxicity. *Clin. Pharmacol. Ther.* **1991**, *50*, 573–579.
- (25) Ratain, M. J.; Rosner, G.; Allen, S. L.; Costanza, M.; Van Echo, D. A.; Henderson, I. C.; Schilsky, R. L. Population pharmacodynamic study of amonafide: A cancer and leukemia group B study. *J. Clin. Oncol.* **1995**, *13*, 741–747.
- (26) Van Quaquebeke, E.; Simon, G.; van den Hove, L.; Kiss, R.; Darro, F. Naphthalimide derivatives, methods for their production and pharmaceutical compositions therefrom. Patents EP2004/447114.2; US60/558,469; PCT/BE2005/000069; WO2005/105753.
- (27) Kiss, R.; de Launoit, Y.; Danguy, A.; Paridaens, R.; Pasteels, J. L. Influence of pituitary grafts or prolactin administrations on the hormone sensitivity of ovarian hormone-independent mouse mammary MXT tumors. *Cancer Res.* **1989**, *49*, 2945–2951.
- (28) Darro, F.; Decaestecker, C.; Gaussin, J. F.; Mortier, S.; Van Ginckel, R.; Kiss, R. Are syngeneic mouse tumor models still valuable experimental models in the field of anticancer drug discovery? *Int. J. Oncol.* **2005**, *27*, 607–616.
- (29) Kraus-Berthier, L.; Jan, M.; Guilbaud, N.; Naze, M.; Pierre, A.; Atassi, G. Histology and sensitivity to anticancer drugs of two human non-small cell lung carcinomas implanted in the pleural cavity of nude mice. *Clin. Cancer Res.* **2000**, *6*, 297–304.
- (30) Mathieu, A.; Rimmelin, M.; D'Haene, N.; Penant, S.; Gaussin, J. F.; Van Ginckel, R.; Darro, F.; Kiss, R.; Salmon, I. Development of a chemoresistant orthotopic human non-small cell lung carcinoma model in nude mice. *Cancer* **2004**, *101*, 1908–1918.
- (31) De Isabelle, P.; Zunino, F.; Capranico, G. Base sequence determinants of amonafide stimulation of topoisomerase II DNA cleavage. *Nucleic Acids Res.* **1995**, *23*, 223–229.
- (32) Zhu, H.; Huang, M.; Yang, F.; Chen, Y.; Miao, Z. H.; Qian, X. H.; Xu, Y. F.; Qin, Y. X.; Luo, H. B.; Shen, X.; Geng, M. Y.; Cai, Y. J.; Ding, J. R16, a novel amonafide analogue, induces apoptosis and G2-M arrest via poisoning topoisomerase II. *Mol. Cancer Ther.* **2007**, *6*, 484–495.
- (33) Pourpak, A.; Landowski, T. H.; Dorr, R. Ethonafide-induced cytotoxicity is mediated by topoisomerase II inhibition in prostate cancer cells. *J. Pharmacol. Exp. Ther.* **2007**, *321* (3), 1109–1117.
- (34) Mayr, C. A.; Sami, S. M.; Dorr, R. T. In vitro cytotoxicity and DNA damage production in Chinese hamster ovary cells and topoisomerase II inhibition by 2-[2'-(dimethylamino)ethyl]-1,2-dihydro-3H-dibenz[de,h]isoquinoline-1,3-diones with substitutions at the 6 and 7 positions (azonafides). *Anticancer Drugs* **1997**, *8*, 245–256.
- (35) Nitiss, J. L.; Zhou, J.; Rose, A.; Hsiung, Y.; Gale, K. C.; Osheroff, N. The bis(naphthalimide) DMP-840 causes cytotoxicity by its action against eukaryotic topoisomerase II. *Biochemistry* **1998**, *37*, 3078–3085.
- (36) Giles, G. I.; Sharma, R. P. Topoisomerase enzymes as therapeutic targets for cancer chemotherapy. *Med. Chem.* **2005**, *1*, 383–394.
- (37) Gong, Y.; Firestone, G. L.; Bjeldanes, L. F. 3,3'-diindolylmethane is a novel topoisomerase II $\alpha$  catalytic inhibitor that induces S-phase retardation and mitotic delay in human hepatoma HepG2 cells. *Mol. Pharmacol.* **2006**, *69*, 1320–1327.
- (38) Zhao, R.; Domann, F. E.; Zhong, W. Apoptosis induced by selenomethionine and methioninase is superoxide mediated and p53 dependent in human prostate cancer cells. *Mol. Cancer Ther.* **2006**, *5*, 3275–3284.
- (39) Li, G. X.; Hu, H.; Jiang, C.; Schuster, T.; Lu, J. Differential involvement of reactive oxygen species in apoptosis induced by two classes of selenium compounds in human prostate cancer cells. *Int. J. Cancer* **2007**, *120*, 2034–2043.
- (40) Pratt, M. A.; White, D.; Kushwaha, N.; Tibbo, E.; Niu, M. Y. Cytoplasmic mutant p53 increases Bcl-2 expression in estrogen receptor-positive breast cancer cells. *Apoptosis* **2007**, *12*, 657–669.
- (41) Kroemer, G.; Jäätelä, M. Lysosomes and autophagy in cell death control. *Nat. Rev. Cancer* **2005**, *5*, 886–897.
- (42) Kondo, Y.; Kanzawa, T.; Sawaya, R.; Kondo, S. The role of autophagy in cancer development and response to therapy. *Nat. Rev. Cancer* **2005**, *5*, 726–734.
- (43) Kanzawa, T.; Germano, I. M.; Komata, T.; Ito, H.; Kondo, Y.; Kondo, S. Role of autophagy in temozolomide-induced cytotoxicity for malignant glioma cells. *Cell Death Differ.* **2004**, *11*, 448–457.
- (44) Okada, H.; Mak, T. W. Pathways of apoptotic and non-apoptotic death in tumour cells. *Nat. Rev. Cancer* **2004**, *4*, 592–603.
- (45) Dimri, G. P.; Lee, X.; Basile, G.; Acosta, M.; Scott, G.; Roskelley, C.; Medrano, E. E.; Linskens, M.; Rubell, I.; Pereira-Smith, O.; Peacocke, M.; Campisi, J. A biomarker that identifies senescent human cells in culture and in aging skin in vivo. *Proc. Natl. Acad. Sci. U.S.A.* **1995**, *92*, 9363–9367.
- (46) Campisi, J. Senescent cells, tumor suppression, and organismal aging: Good citizens, bad neighbors. *Cell* **2005**, *120*, 513–522.
- (47) Chang, B. D.; Broude, E. V.; Dokmanovic, M.; Zhu, H.; Ruth, A.; Xuan, Y.; Kandel, E. S.; Lausch, E.; Christov, K.; Roninson, I. B. A senescence-like phenotype distinguishes tumor cells that undergo terminal proliferation arrest after exposure to anticancer agents. *Cancer Res.* **1999**, *59*, 3761–3767.
- (48) Brana, M. F.; Ramos, A. Naphthalimides as anti-cancer agents: Synthesis and biological activity. *Curr. Med. Chem. Anticancer Agents* **2001**, *1*, 237–255.
- (49) Brana, M. F.; Cacho, M.; Garcia, M. A.; de Pascual-Teresa, B.; Ramos, A.; Acero, N.; Llinares, F.; Munoz-Mingarro, D.; Abradelo, C.; Rey-Stolle, M. F.; Yuste, M. Synthesis, antitumor activity, molecular modeling, and DNA binding properties of a new series of imidazonaphthalimides. *J. Med. Chem.* **2002**, *45*, 5813–5816.
- (50) Bailly, C.; Carrasco, C.; Joubert, A.; Bal, C.; Watez, N.; Hildebrand, M. P.; Linsiaux, A.; Colson, P.; Houssier, C.; Cacho, M.; Ramos, A.; Brana, M. F. Chromophore-modified bisnaphthalimides: DNA recognition, topoisomerase inhibition, and cytotoxic properties of two mono- and bisfuronaphthalimides. *Biochemistry* **2003**, *42*, 4136–4150.
- (51) Brana, M. F.; Cacho, M.; Ramos, A.; Dominguez, M. T.; Pozuelo, J. M.; Abradelo, C.; Rey-Stolle, M. F.; Yuste, M.; Carrasco, C.; Bailly, C. Synthesis, biological evaluation and DNA binding properties of novel mono and bisnaphthalimides. *Org. Biomol. Chem.* **2003**, *1*, 648–654.
- (52) Brana, M. F.; Cacho, M.; Garcia, M. A.; de Pascual-Teresa, B.; Ramos, A.; Dominguez, M. T.; Pozuelo, J. M.; Abradelo, C.; Rey-Stolle, M. F.; Yuste, M.; Banez-Coronel, M.; Lacal, J. C. New analogues of amonafide and elinafide, containing aromatic heterocycles: Synthesis, antitumor activity, molecular modeling, and DNA binding properties. *J. Med. Chem.* **2004**, *47*, 1391–1399.
- (53) Lefranc, F.; Kiss, R. Autophagy, the Trojan horse to combat glioblastomas. *Neurosurg. Focus* **2006**, *20*, E7.
- (54) Lefranc, F.; Brotchi, J.; Kiss, R. Possible future issues in the treatment of glioblastomas: special emphasis on cell migration and the resistance of migrating glioblastoma cells to apoptosis. *J. Clin. Oncol.* **2005**, *23*, 2411–2422.
- (55) Mathieu, V.; Le Mercier, M.; De Neve, N.; Sauvage, S.; Gras, T.; Roland, I.; Lefranc, F.; Kiss, R. Galectin-1 knockdown increases sensitivity to temozolomide in a B16F10 mouse metastatic melanoma model. *J. Invest. Dermatol.* **2007**, in press.
- (56) Stupp, R.; Mason, W. P.; van den Bent, M. J.; Weller, M.; Fisher, B.; Taphoorn, M. J.; et al. Radiotherapy plus concomitant and adjuvant Temozolomide for glioblastoma. *N. Engl. J. Med.* **2005**, *352*, 987–996.

- (57) Giovannetti, E.; Mey, V.; Nannizzi, S.; Pasqualetti, G.; Del Tacca, M.; Danesi, R. Pharmacogenetics of anticancer drug sensitivity in pancreatic cancer. *Mol. Cancer Ther.* **2006**, *5*, 1387–1395.
- (58) Westphal, S.; Kalthoff, H. Apoptosis: Targets in pancreatic cancer. *Mol. Cancer* **2003**, *2*, 6.
- (59) Joseph, B.; Darro, F.; Behard, A.; Lesur, B.; Collignon, F.; Decaestecker, C.; Frydman, A.; Guillaumet, G.; Kiss, R. 3-Aryl-2-quinolone derivatives: synthesis and characterization of in vitro and in vivo antitumor effects with emphasis on a new therapeutical target connected with cell migration. *J. Med. Chem.* **2002**, *45*, 2543–2555.
- (60) Delfourne, E.; Darro, F.; Portefaix, I.; Galaup, C.; Bayssade, S.; Bouteillé, A.; Le Corre, L.; Bastide, J.; Collignon, F.; Lesur, B.; Frydman, A.; Kiss, R. Synthesis and in vitro antitumor activity of novel ring D analogues of the marine pyridoacridine ascididemin: Structure-activity relationship. *J. Med. Chem.* **2002**, *45*, 3765–3771.
- (61) Van Quaquebeke, E.; Simon, G.; Andre, A.; Dewelle, J.; Yazidi, M. E.; Bruyneel, F.; Tuti, J.; Nacoulma, O.; Guissou, P.; Decaestecker, C.; Braeckman, J. C.; Kiss, R.; Darro, F. Identification of a novel cardenolide (2'-oxovorusharin) from *Calotropis procera* and the hemisynthesis of novel derivatives displaying potent in vitro antitumor activities and high in vivo tolerance: Structure-activity relationship analyses. *J. Med. Chem.* **2005**, *48*, 849–856.
- (62) Ingrassia, L.; Nshimyumukiza, P.; Dewelle, J.; Lefranc, F.; Wlodarczak, L.; Thomas, S.; Dielie, G.; Chiron, C.; Zedde, C.; Tisnès, P.; van Soest, R.; Braeckman, J. C.; Darro, F.; Kiss, R. A lactosylated steroid contributes in vivo therapeutic benefits in experimental models of mouse lymphoma and human glioblastoma. *J. Med. Chem.* **2006**, *49*, 1800–1807.
- (63) Lesueur-Ginot, L.; Demarquay, D.; Kiss, R.; Kasprzyk, P. G.; Dassonneville, L.; Bailly, C.; Camara, J.; Lavergne, O.; Bigg, D. C. Homocamptothecin, an E-ring modified camptothecin with enhanced lactone stability, retains topoisomerase I-targeted activity and anti-tumor properties. *Cancer Res.* **1999**, *59*, 2939–2943.
- (64) Mijatovic, T.; Op De Beeck, A.; Van Quaquebeke, E.; Dewelle, J.; Darro, F.; de Launoit, Y.; Kiss, R. The cardenolide UNBS1450 is able to deactivate nuclear factor-kappaB-mediated cytoprotective effects in human non-small cell lung cancer cells. *Mol. Cancer Ther.* **2006**, *5*, 391–399.

JM070315Q